Received: 19 December 2023 | Accepted: 31 March 2024

DOI: 10.1002/jmv.29620

RESEARCH ARTICLE

JOURNAL OF MEDICAL VIROLOGY WILEY

Pan-microscopic examination of monkeypox virus in trophoblasts cells reveals new insights into virions release through filopodia-like projections

Jonatane Andrieu[1] | Margaux Valade[2] | Marion Lebideau[2] | Florence Bretelle[2,3] | Jean-Louis Mège[1,4] | Nathalie Wurtz[2] | Soraya Mezouar[1] | Bernard La Scola[2] | Jean-Pierre Baudoin[2]

[1]Centre National de la Recherche Scientifique, Établissement Français du Sang, Anthropologie bio-culturelle, Droit, Éthique et Santé, Aix-Marseille University, Marseille, France

[2]Institut Recherche Développement, Assistance Publique—Hôpitaux de Marseille, Microbe, Evolution, Phylogeny Infection, Aix-Marseille University, Marseille, France

[3]Département de gynécologie et d'obstétrique, Gynépole, La Conception, AP-HM, Marseille, France

[4]Laboratoire d'Immunologie, Assistance Publique Hôpitaux de Marseille (APHM), Marseille, France

Correspondence

Bernard La Scola and Jean-Pierre Baudoin, Institut Recherche Développement, Assistance Publique—Hôpitaux de Marseille, Microbe, Evolution, Phylogeny Infection, Aix-Marseille University, PU-PH, 19-21, Blvd. Jean Moulin, 13385 Marseille, France.
Email: bernard.la-scola@univ-amu.fr, jpbaudoin@live.fr and jean-pierre.baudoin@ap-hm.fr

Abstract

Vertical transmission has been described following monkeypox virus (MPXV) infection in pregnant women. The presence of MPXV has been reported in the placenta from infected women, but whether pathogens colonize placenta remains unexplored. We identify trophoblasts as a target cell for MPXV replication. In a pan-microscopy approach, we decipher the specific infectious cycle of MPXV and inner cellular structures in trophoblasts. We identified the formation of a specialized region for viral morphogenesis and replication in placental cells. We also reported infection-induced cellular remodeling. We found that MPXV stimulates cytoskeleton reorganization with intercellular extensions for MPXV cell spreading specifically to trophoblastic cells. Altogether, the specific infectious cycle of MPXV in trophoblast cells and these protrusions that were structurally and morphologically similar to filopodia reveal new insights into the infection of MPXV.

KEYWORDS

infectious diseases, microscopy, monkeypox virus, placenta, poxvirus, pregnancy, trophoblast

1 | INTRODUCTION

Monkeypox (MPX) is a zoonotic viral infection that induces a smallpox-like rash, caused by the monkeypox virus (MPXV). MPXV belongs to the poxviruses family, *Poxviridae*, including variola virus, the causative agent for infamous smallpox disease associated to millions of deaths throughout the history.[1] The incubation period for MPX disease is 7–14 days, beginning with a 1- to 4-day prodrome of fever, headache, and muscle pain, with sometime swelling of the lymph nodes. Lymphadenopathy may be accompanied by exhaustion, chills, backache, sore throat, and general

malaise. The appearance of lesions accompanied by skin or mouth eruptions and/or pustules (macular, papular, vesicular, or pustular) alters the epithelial cell layers of the skin. The rash first appears as macules, followed by papules, vesicles, and pustules, before crusting over after 7–14 days.[2–4] All the symptoms are often mild, but can also be fatal as in smallpox.[1] Recently, the increase in MPXV cases around the world is raising a global concern about the emergence of a potential pandemic. During the latest MPX epidemic, the symptoms described in several report cases highlight the presence of a broad spectrum of cutaneous/mucosal manifestations, mainly anogenital, but also oropharyngeal involvement, and most infected patients reported prodromal signs/symptoms (fever, asthenia, and lymphadenopathy) before the rash.[5–7] Varying in size from 130 to 450 kb,[8] poxviruses are viruses wrapped with a double-stranded DNA genome.[9] Within the host cell, poxviruses assemble within the cytoplasmic where various virion assembly intermediates such as immature, mature, and extracellular wrapped states are found. In the mature state, poxviruses have an ovoid morphology with a size of 220–450 nm and 140–260 nm in length and width, respectively. At the level of the membrane of the mature virion, a tubular assembly of proteins, lateral bodies, and at the level of its biconcave nucleus is the nucleoprotein and DNA. The acquisition of additional membrane of the trans-Golgi cisternae or plasma membrane causes a change in the state of the virion which becomes wrapped and or wrapped extracellular. Current data on virion morphology are due to transmission electronic microscopy.[10–15]

Vertical transmission and pregnancy loss have been described following MPXV infection.[16] Although trophoblasts, the epithelial cells of the placenta, are highly resistant to infection, MPXV is able to cross the placental barrier using endocytic pathways commonly used by viruses for entry, such as clathrin- or caveolae-mediated pathways.[17] MPXV infection during pregnancy can lead to premature delivery and even fetal death. Fetal death has been reported in several cases to be accompanied by morphological changes in the placenta, consisting of necrotic villi and large amounts of fibrin deposits, with hemorrhages in the placental villi.[18]

Although electron microscopy has provided a better understanding of the cellular infection mechanisms of MPXV by investigating biopsies from animal[19] or human,[10,12,13] and in vitro cell lines,[14,15] the exact mechanisms by which orthopoxviruses cross the placenta during pregnancy have yet to be characterized.[20] Interestingly, one hypothesis for the vertical transmission of MPXV to the fetus in pregnant women is that MPXV could originate from the vagina or maternal bloodstream to infect placental syncytiotrophoblasts via transcytosis or fusion with the trophoblast membrane.[20,21]

Understanding the virus–cell interactions is key to vaccines, treatments, and diagnoses. Our study highlights the evolution of MPXV infection in placenta. Using placental explants, we demonstrated that trophoblasts represent a target cell for MPXV. In a pan-microscopy approach, using different microscopy techniques, we decipher the specific infectious cycle of hMPXV and inner cellular structures in trophoblasts. The results revealed the formation of a specialized region for viral morphogenesis and replication, and infection-induced cellular remodeling. We also reported intercellular extensions for MPXV cell spreading specifically to trophoblastic cells. This study offers new insights into the infection of MPXV.

2 | MATERIAL AND METHODS

2.1 | Ethic statement

The protocol of the study to collect at term-placenta just after delivery was approved by an independent national review board (ethic number 08-12). All pregnant women were recruited at the Gynecology-Obstetrics Department of the "Hôpital de la Conception" (Marseille, France) and provided written informed consent. The manipulation of the MPXV strain and its nucleic acids was carried out according to ANSM ("Agence National de Securité du medicament et des produits de Santé"), authorization AMO-168522023.

2.2 | Cell culture

Cell lines, Vero E6 green-monkey kidney cell line (ATCC® CRL-1586™), were cultivated in minimum essential medium (MEM; Gibco) supplemented with 10% fetal calf serum (FCS) and 1% L-glutamine (M10 medium). JEG-3 placenta choriocarcinoma cell line (ATCC HTB-36) was cultivated in Dulbecco's modified Eagle medium (DMEM; Gibco) supplemented with 10% (v/v) fetal bovine serum (FBS; Sigma-Aldrich), 2 mM glutamine (Gibco).

Vero E6 and JEG-3 cells were cultivated using a specific matrix. Briefly, substrate preparation was performed by Cell and Soft. Briefly, Greiner Bio-One 96-well single-break strip microplates (Greiner Bio-One) were ultraviolet (UV) sterilized at 365 nm (125 mW/cm^2) (UV-KUB 1) for 5 min under a laminar flow hood. Collagen coating was then performed under a sterile laminar flow cabinet. Subsequently, 400 ng of rat tail collagen I (Corning Life Science) was added to each well and incubated at 37°C overnight. Plates were stored at 4°C until used at our laboratory. Then, 2×10^5 cells/mL (200 µL) of both cells' suspension was distributed into each modular well of two removable single-break strips (eight wells each) in a microplate and incubated for 24 h at 37°C with 5% CO_2.

Primary cells. Trophoblasts were isolated from the tissue of healthy placenta. Entire placenta tissues were digested in Hank's Balanced Salt Solution (HBSS; Life Technologies), DNase I 2.5 mM and 2.5% trypsin (Life Technologies). Cell suspension was filtered through 100-µm pores and deposited on a Percoll density gradient (GE Healthcare) and centrifuged at 1200×*g* for 20 min. Trophoblasts were then selected using magnetic beads (rat anti-mouse; Miltenyi Biotec) coated with anti-EGFR (epidermal growth factor receptor) antibodies (Santa Cruz Biotechnology). The isolated trophoblasts were cultured in DMEM F-12 medium (Life Technologies) supplemented with 10% FBS at 37°C in the presence of 5% CO_2.

2.3 | Virus culture and cell infection

The IHUMPXV8 strain was the eighth isolated in our laboratory from a rectal swab of a man infected during the 2022 monkeypox epidemic in Marseille (France). Three passages in Vero E6 cells were required for the production and strains were then stored at −80°C. The second strip was used as a negative control by adding 50 µL of the M4 medium only and both strips were centrifuged at 2272×*g* for 1 h at 37°C. The supernatant from the wells was discarded, the cells rinsed gently three times with M4 medium and 200 µL of M4 medium was added to the 8 wells. Cells were incubated at 37°C and 5% CO_2.

Vero E6 and JEG-3 cell monolayers were infected in one of the two strips by removing culture medium and adding 50 µL of MPXV viral suspension (IHUMPXV8 strain) (MOI 1) in the MEM medium supplemented with 4% FCS and 1% L-glutamine (M4 medium) or DMEM (Gibco) supplemented with 10% (v/v) FBS, 2 mM glutamine. For each postinfection time point (2, 4, 18, 24, 48, 72, and 96 h), one infected and one noninfected modular well was fixed by adding 200 µL of 2.5% glutaraldehyde in 0.1 M sodium cacodylate buffer and stored at 4°C until infectious cycle.

2.4 | Culture and infection of placental tissue

About 1 cm^2 pieces of placenta were taken off between the umbilical cord implantation and the margin of the placenta, including the maternal and fetal sides. Biopsies were rinsed with phosphate-buffered saline (PBS), cut into about 4 mm^2 pieces, and then transferred to six-well plates containing DMEM F-12, 10% FBS, 100 units/mL of penicillin, and 100 µg/mL streptomycin at 37°C overnight. Explants were infected with 1×10^5 plaque-forming units (PFU)/explant during 24 h, as previously reported.[22–24] Tissues were then harvested, fixed in 4% formaldehyde for 24 h, dehydrated and embedded in paraffin. After deparaffinization, permeabilization by 0.1% Triton X-100 and blocking step consisting of 10% FBS, 2-µm tissue sections were incubated with primary human IgG1 anti-Monkeypox-A35R (A3R-M575; ACRObiosystems) at 1/250 dilution in H_2O for 1 h. Labeled cells were then washed twice with FBS 0.1% in H_2O for 5 min. Second incubation with secondary anti-human Alexa-488 secondary antibody (RA-11013; Thermo-Fischer Scientific) at 1/250 dilution in H_2O and DAPI, phalloidin-555 for 1 h, and washed for 5 min with FBS 0.1% in H_2O. For all steps above, the incubation was done at room temperature (RT). Coverslips with placenta explants were mounted on microscope slides with mowiol (F4680, Sigma).

2.5 | Viral DNA extraction and quantitative polymerase chain reaction

Viral DNA was extracted using EZ1 advanced XL with virus mini kit v2.0 (Qiagen). Virus detection was performed using program for viral quantitative polymerase chain reaction (Figure S10 and Table 1). The G2 gene was investigated for the MPXV detection (Figure S10 and Table 2).

TABLE 1 Program used for viral quantitative polymerase chain reaction.

Steps	Temperature (°C)	Time	Cycles
Initial denaturation	95	10 min	1
Denaturation	95	10 s	45
Hybridization/elongation	60	30 s	
Cooling	37	5 s	1

TABLE 2 Primers used for monkeypox virus detection.

Primers	Sequences
G2R_F	GGAAAGTGTAAAGACAACGAATACAG
G2R_R	GCTATCACATAATCTGGAAGCGTA
G2R_P	6FAM-AAGCCGTAATCTATGTTGTCTATCGTGTCC

2.6 | Cell viability

Cell viability was evaluated using the 3-[4,5-dimethylthiazol-2-yl] −2,5 diphenyl tetrazolium bromide (MTT) assay (Thermofisher). After 24, 48, 72, and 96 h of MPXV stimulation, 10 µL of MTT (5 mg/mL; Sigma-Aldrich) were added to the cell cultures and incubated at 37°C for 4 h. The formed formazan crystals were solubilized with 50 µL of dimethylsulphoxide (DMSO) for 30 min at 37°C and quantified using a Tecan infinite 200 plate reader at 570 nm (Tecan©).

2.7 | Transmission electron microscopy (TEM) of MPXV-infected cells monolayers ultra-thin sections

For electron microscopy, virus-infected cell cultures in microplates were processed according to Le Bideau et al.[25] Cells were fixed with glutaraldehyde (2.5%) in 0.1 M sodium cacodylate buffer. Resin embedding was microwave-assisted with a PELCO BiowavePro$^+$ (Ted Pella Inc), by exchanging 200 µL of the different solutions at each step. Samples were washed two times with a mixture of 0.2 M saccharose/0.1 M sodium cacodylate and postfixed with 1% OsO4 diluted in 0.2 M potassium hexa-cyanoferrate (III)/0.1 M sodium cacodylate buffer. After two washes with distilled water, samples were gradually dehydrated by successive baths in 30%, 50%, 70%, 90%, 96%, and 100% ethanol. Substitution with Epon resin (Embed 812 mixed with NMA, DDSA, and DMP-30 hardener; Electron Microscopy Sciences) was achieved by incubations with 25%, 50%, 75% Epon resin in ethanol and incubations with 100% Epon resin. Polymerization was done in 100% fresh Epon for 72 h at 60°C. All solutions used above were 0.2 µm filtered. Resin blocks were placed in a UC7 ultramicrotome (Leica Biosystems), trimmed to pyramids, and ultrathin 100 nm sections were cut and placed on HR25 300 Mesh Copper/Rhodium grids (TAAB; Reading). Sections were contrasted according to Reynolds. Electron micrographs were

obtained on a Tecnai G2 TEM (Thermo-Fischer/FEI) operated at 200 keV equipped with a 4096 × 4096 pixels resolution Eagle camera (FEI).

2.8 | Scanning electron microscopy (SEM) of whole MPXV-infected JEG-3 cells monolayers

For SEM of whole infected cells or placental explants, samples were fixed with glutaraldehyde 2.5% in 0.1 M cacodylate buffer, and then processed in 1-min steps: washing with 0.1 M cacodylate buffer, washing with distilled water, dehydration with ethanol 50% and ethanol 100%, incubation with a mixture 100% ethanol/100% hexamethyldisilazane (HDMS) in a 1:2 ratio and finally with 100% of HDMS. After HDMS depletion samples were finally air-dried for 1 h and platinum sputter-coated for 20 s at 10 mA (Hitachi MC1000). The observation was made using a SU5000 (Hitachi High-Technologies) SEM with an SE detector at 1 kV acceleration voltage or BSE detector at 15 kV acceleration voltage, in high-vacuum and observation (spot size 30) mode.

2.9 | Immunofluorescence

Primary and cell line trophoblasts (5×10^5 cells/well) were cultured into a 24-well plate containing a glass coverslip in shell vials and ± infected with MPXV virus were fixed at different times postinfection with paraformaldehyde 4% for 15 min at RT. After then permeabilized with 0.1% Triton X-100 in PBS for 3 min. Permeabilized cells were incubated with blocking buffer (3% FBS diluted in PBS) for 30 min. Cells were incubated with primary human IgG1 anti-Monkeypox-A35R (A3R-M575; ACROBiosystems) at 1/250 dilution in H_2O for 1 h. Labeled cells were then washed twice with FBS 0.1% in H_2O for 5 min. Second incubation with secondary anti-human Alexa-488 secondary antibody (RA-11013; Thermo-Fischer Scientific) at 1/250 dilution in H_2O and DAPI, phalloidin-555 for 1 h, and washed for 5 min with FBS 0.1% in H_2O. For all steps above, the incubation was done at RT. Coverslips with immunostained placenta cells were mounted on microscope slides with mowiol (F4680; Sigma).

2.10 | Confocal laser scanning microscopy (CLSM)

CLSM of placental explants and trophoblast cells was performed with an inverted LSM800 (Zeiss) microscope. Acquisitions were performed with × 63 objective and a zoom between 0.5 and 2.7. Image size was 1024 × 1024 pixels. For the DAPI stain, Alexa-488, Alexa-555 and Alexa-647 fluorophores imaging, 405, 556, and 640 nm lasers were used, respectively. Either maximal orthogonal Z-projections from the Z-stacks or single planes were used for analysis. In Figure 7, colors were inverted for Alexa-488 and Alexa-555 fluorophores.

2.11 | Statistics

Statistical analysis was performed with GraphPad Prism, using the one-way analysis of variance (ANOVA) with Tukey's post hoc test for multiple comparisons, and statistical significance was considered for p values below 0.05. Details for individual analyses are provided in the figure legend. Unless otherwise noted, data are presented as mean ± standard deviation. The graphical abstract was drawn up using Biorender (acceptance number for publication, ND26HG48Y0).

3 | RESULTS

3.1 | Trophoblast is a target cell for MPXV

We first wondered if trophoblasts are a target for MPXV. We used placental explants from healthy pregnant women that we incubated ex vivo with MPXV. From 24 to 72 h postinfection (p.i.), we did not observe macroscopic alteration of the architecture of the tissue. The staining with anti-MPVX was distributed thought the tissue (Figure 1A). At 24 h p.i., we observed a fairly peripheral infection of the placenta tissue with the presence of the virus in cytokeratin 7 (CTK7) positive trophoblasts (extra-villous trophoblasts) (Figure 1A, A1–A4). Forty-8 h p.i., we observed a more diffuse infection of the placenta tissue, with many more particles observable within the tissue (Figure 1A, A5–A6) suggesting that MPXV is able to cross the syncytial barrier targeting villous cytotrophoblasts (VCT) (Figure 1A, A6). Finally, at 72 h, we still observed diffuse infection in the tissue with syncytium detachment (Figure 1A, A7–A10) suggesting that long-term MPXV infection induces loss of tissue homogeneity and detachment of syncytium cells, while ensuring replication of the virus in the tissue. Interestingly, we also observed CTK7-positive trophoblast making extensions with viral particle inside (Figure 1A, A7–A10). This effect of syncytium detachment can also be seen by SEM with observations of placental explants at 72 h postinfection. Indeed, we observed a visual difference in placental tissue infected with MPXV, with areas of detachment and tissue degradation caused by the infection (Figure 1B2, white arrow), in contrast to healthy tissue, which remained homogeneous and intact throughout (Figure 1B1, white arrow). Hence, trophoblasts can be infected by MPXV in placenta microenvironment.

We then isolated trophoblasts from placenta from healthy pregnant women and incubated them ex vivo with MPXV. The level of infection and replication increased over time from 24- to 96-h postinfection (Figure 1C). Moreover, their viability decreases drastically from 48 h p.i. to less than 20% viability 96 h p.i. (Figure 1C) suggesting that trophoblast could be a niche for MPVX replication.

3.2 | Ultrastructural features of MPXV infectious cycle in trophoblast cell line

To visualize the replication of MPXV in trophoblast, we used the JEG-3 cell line as model as previously reported.[26–28] In a first step,

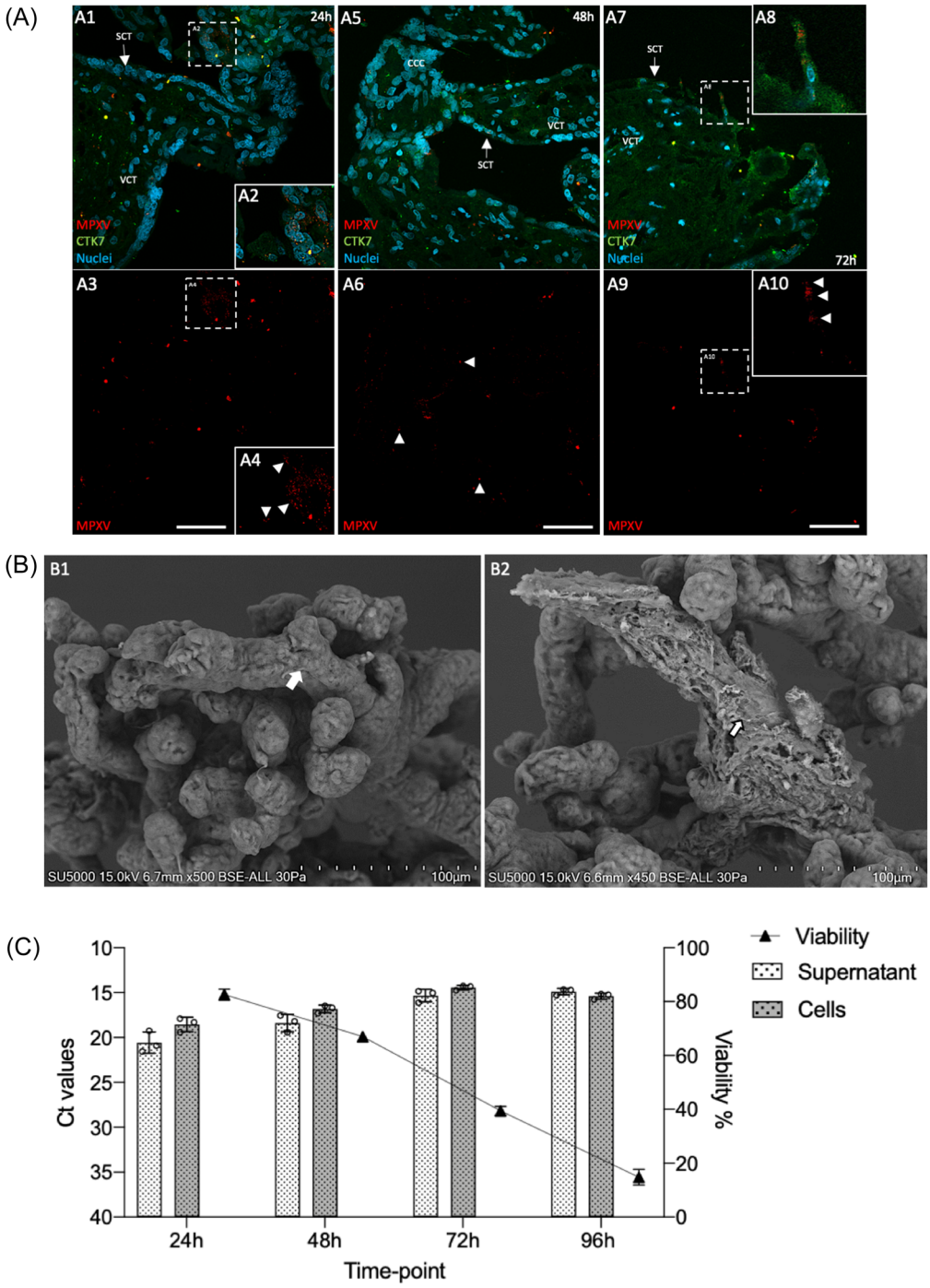

FIGURE 1 MPXV infection of placental tissue. (A) Immunofluorescence was performed on paraffin sections of placental explants, infected with MPXV ex vivo over a kinetic time course. At 24 h infection in placental tissue remains peripheral, with little dissemination within the tissue, and is mainly located in syncytiotrophoblasts (A1–A3). At 48 h, infection is diffuse, with localized particles in and around the placental tissue (A5–A6). At 72 h the placental barrier begins to de-epithelialize-like and lose its compact structure, with several MPXV particles visible in its ramifications (A7–A10). (B) Scanning electron microscopy of placental tissue at 72 h under unstimulated (B1) and monkeypox-infected conditions (B2). X500-450 magnification. (C) Graphical representation of virus quantity (Ct-values) of MPXV-infected primary trophoblast cells supernatant and cells over time (left axis). In parallel, percentage of viability of MPXV-infected primary trophoblast cells over time (right axis). Data values represent three healthy donors different with the mean ± standard error of the mean from one manipulation in triplicates. MPXV, monkeypox virus.

we confirmed infection, replication, and viability in the JEG-3 trophoblast line, as in primary trophoblasts and we found that trophoblast JEG-3 cells had a profile similar to that of primary trophoblasts (Figure S10). Alteration of trophoblastic cells in the monolayers was directly observed by SEM. At the time of MPXV infection (30 min and 2 h) there was no alteration of the cell confluence (Figure 2A,B). At 24 h p.i., there was the appearance of both cell-free and necrotic zones (Figure 2C). These areas were increasingly present with the increase in infection time especially at 48 (Figure 2D), 72 (Figure 2E), and 96 h (Figure 2F) p.i.

Secondly, we investigated the MPXV replication in JEG-3 cells over time using transmission electron microscopy (TEM) on ultra-thin sections after fixation of the cells at successive time points p.i. For comparison, we studied in parallel for the same time points MPXV–infected Vero E6 cells, a green-monkey kidney cell line representing a classical model for in vitro studies of virus infectious cycles.[14] We used in our following morphological description the same nomenclature as the one used in,[14] and thanks to our analysis of successive time points p.i., we were able to link the previously published observations[14] to specific time points during MPXV infectious cycle.

At early time point (30 min p.i.), mature extracellular MPXV viral particles could be observed, binding to the cell's plasma membrane of JEG-3 cells (Figure 3A1–A2). The shape of the JEG-3 cell nuclei was circular, and cells contained abundant glycogen granules (Figure 3A1–A2). Observed MPXV particles were morphologically consistent with the literature,[12–15] possessing the typical oval coffee bean or brick shape containing an external membrane and biconcave core. Mean longest and smallest diameters were 274 ± 35 and 193 ± 31 nm (n = 48), and 305 ± 25 and 220 ± 24 nm (n = 14), for oval coffee bean and brick-shaped particles, respectively. In Vero E6 cells, MPXV virions were found free extracellularly between cells, attached to the cell plasma membranes (Figure S1). When very close to the cell plasma membranes, virions were located between cell microvilli, sometimes facing presumptive nascent clathrin-coated endocytosis vesicles (Figure S1). We also observe virions located inside forming endocytic vesicles (Figure S1) in Vero E6 cells, as well as internalized particles in intracellular vacuoles, mixed with membranous material. Internalized particles had different morphologies: full particles with protruding material that may correspond to particles delivering their content to the vacuoles or the cytoplasm (E), or flattened particles (F–H) that may correspond to particles after cell delivery (Figure S1). In comparison, intracellular MPXV particles were observed in JEG-3 cells 1-h p.i. (Figure 3B,C). Thus, MPXV particles cell internalization seemed to be slightly delayed in JEG-3 cells compared to Vero E6 cells.

Two hours p.i., MPXV-like particles were depicted inside endocytic vesicles in the JEG-3 cells cytoplasm (Figure 3D–F). Mixed with the MPXV virions in the endocytic compartment's electron-dense membranes were also present, which may correspond to degraded MPXV virions. Glycogen granules were abundant (Figure 3D) and nuclei were round (Figure 3E). In Vero E6 cells, similar observations were made with MPXV-like particles found trafficking in the cell cytoplasm inside endocytic vesicles (Figure S2). Larger compartments containing numerous membranes, which may correspond to degraded virions, were also observed close to the nuclei (Figure S2).

There was no clear signature of either immature (IV) or mature (IMV) virions in JEG-3 cells between 2 and 18 h p.i. (data not shown), period that probably represented the "eclipse phase" of the JEG-3

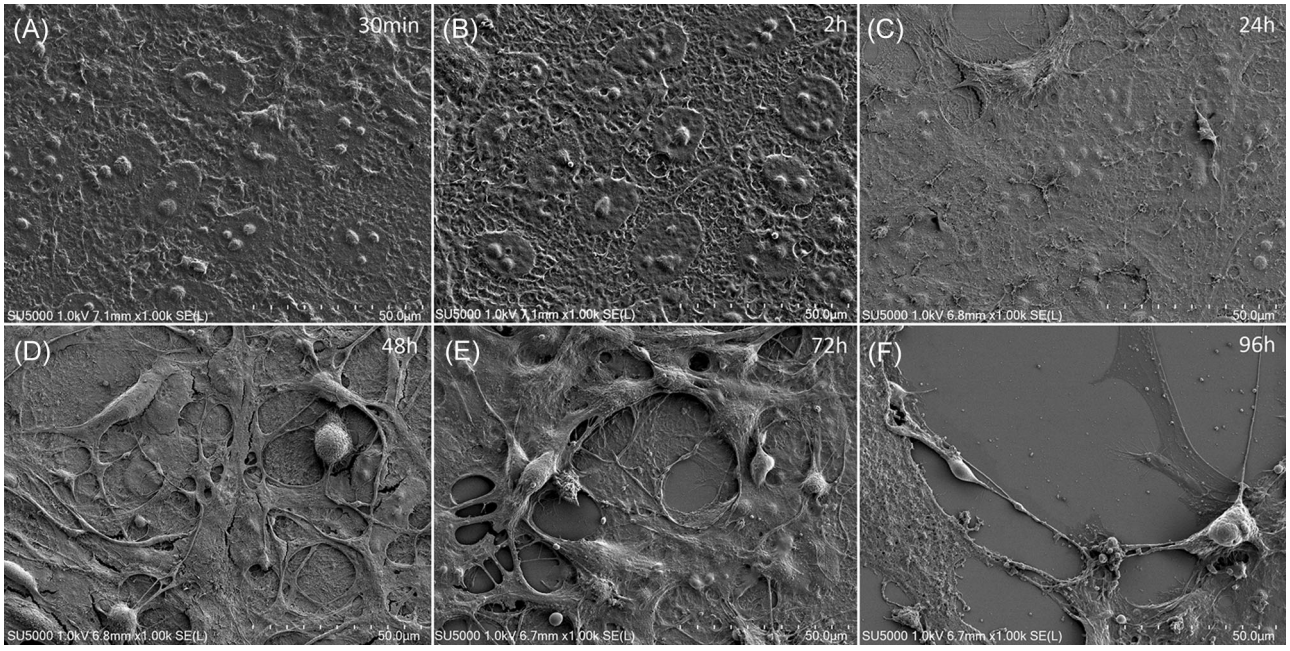

FIGURE 2 Exploration of the trophoblast JEG-3 cells following MPXV infection over time by scanning electron microscopy. Scanning electron microscopy of whole-mount MPXV infected trophoblast JEG-3 cell monolayers at 30 min (A), 2 h (B), 24 h (C), 48 h (D), 72 h (E), and 96 h (F) postinfection time points (×1000 magnification). MPXV, monkeypox virus.

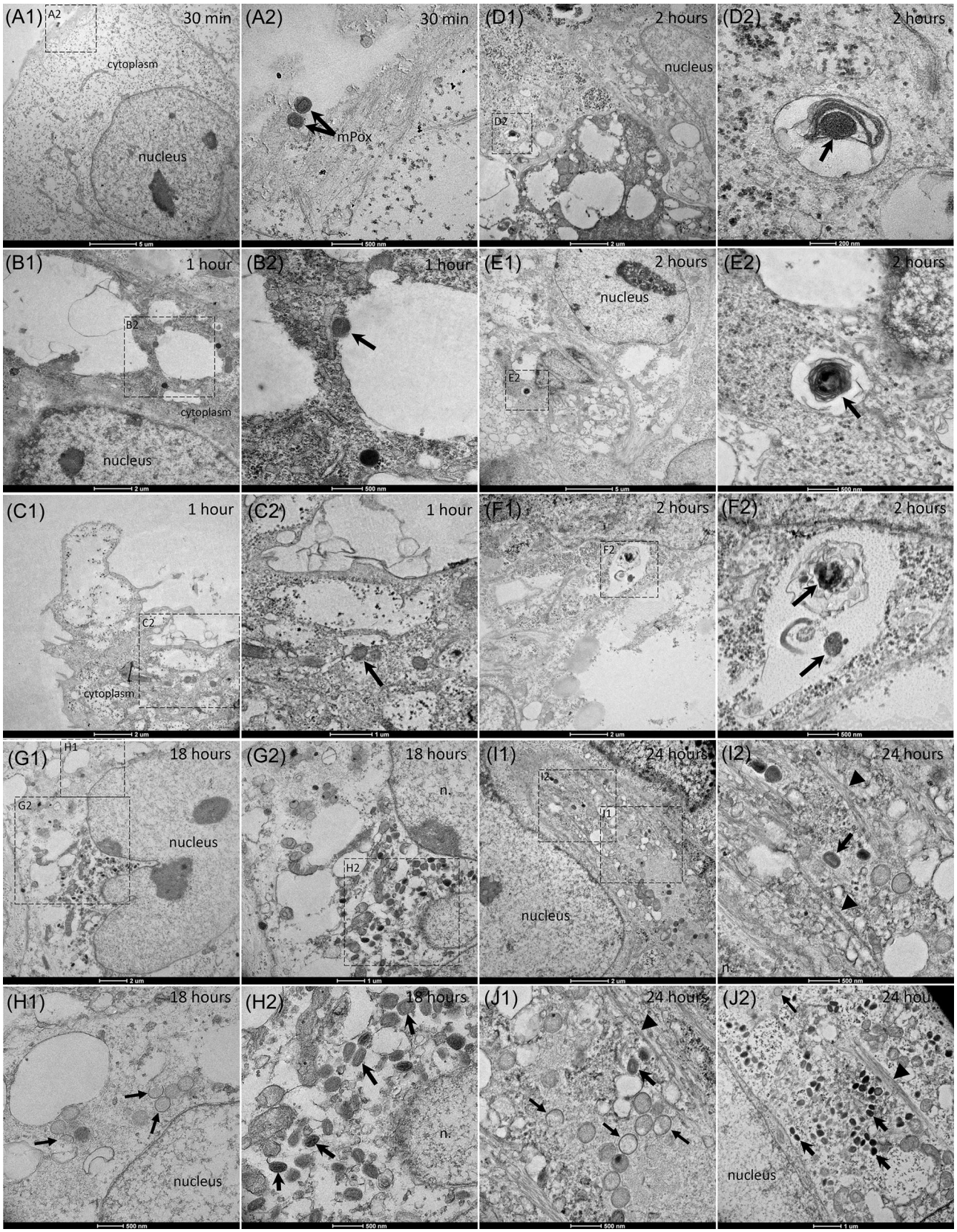

FIGURE 3 (See caption on next page).

cells. Eclipse phase for Vero E6 cells was shorter, with no clear morphological signature of infection at 5 and 8 h p.i., and no observation of intact uptaken or forming virion. We nevertheless noticed an increase in glycogen granules contained in the Vero E6 cells (data not shown). At 13 h p.i., a very few viral crescents corresponding to the first stage of virions assembly were observed inside Vero E6 cells, as well as a few "mini-nuclei"[14] (data not shown).

MPXV virus replication was clearly depicted in JEG-3 cells 18 h p.i., with "crescent-shaped" particles, immature (IV), and mature (IMV) particles (Figure 3G1–H2). JEG-3 cells nuclei were often observed possessing invaginations, with mature (IMV) particles concentrated at the level of these nuclei indentations, while virus replication factories were found more distantly from the nuclei in cell cytoplasm (Figure 3G1–H2). At the same time, glycogen granules were less abundant than at earlier time points, with sparse granules disseminated in cell cytoplasm (Figure 3G1–H2). In Vero E6 cells, immature virus (IV) as well as mature particles (IMV) were also detected at 18 h p.i. (Figure S3).

At 24 h p.i., MPXV replication was very active in JEG-3 cells, with numerous immature (IV) and mature (IMV) particles (Figure 3I,J). Nuclear invaginations were more pronounced than at earlier 18 h p.i., and actin microfilament bundles were present at the level of nuclei indentations, between IV and IMV particles (Figure 3I2–J2). Vacuoles were also more often present in the MPXV-infected JEG-3 cells at 24 h than at 18 h p.i. (Figure 3I,J). In Vero E6 cells, the replication of the virus progressed at 24 h p.i. with more abundant IV particles (Figure S4). In parallel, Vero E6 cells formed large vacuoles.

From 48 h p.i., characteristic ultrastructural features of cell lysis were seen for some MPXV-infected JEG-3 cells, with disorganized plasma cell membranes and dispersed cytoplasm (Figure 4). Mature MPXV particles were also depicted in the extracellular space between cells in the monolayers (Figure 4). In comparison, no sign of cell lysis was observed in Vero E6 cells, albeit vacuolization of the Vero E6 cells at 48 h p.i. was more pronounced than 1 day earlier. MPXV virus production increased in Vero E6 cells with IV predominantly located at cell centers, close to the nuclei, while IMV was located more at cell periphery (Figure S5).

Seventy-2 h p.i., lysis of JEG-3 cells was more pronounced than at 48 h p.i., with highly disorganized cells with a loose cytoplasm and numerous vacuoles containing numerous mature IMV particles (Figure 5A,B). Immature IV particles were not present at 72 h p.i., suggesting that cellular disorganization impaired viral replication at late p.i. times. In contrast, Vero E6 cells had no signs of cell lysis, with round-shaped cells containing asymmetric IV versus IMV MPXV particles distribution, from the center toward the periphery (Figure S6).

At 96 h p.i., the few remaining JEG-3 cells that we could observed were highly disorganized, with numerous vacuoles and mature IMV particles about to be released (Figure 5C,D). Similarly, 96 h p.i., a very few intact Vero E6 cells remained in the monolayers, and these cells contained very large vacuoles. As for JEG-3 cells, most of the cells were lyzed, with cell ghosts containing numerous IMV mature particles (Figure 5C,D).

3.3 | Remodeling of trophoblast cells following MPXV infection

To characterize the effect of MPXV infection on JEG-3 cells monolayers morphology, at the cellular level, we performed a whole-mount analysis by SEM (MEB). At 30 min (Figures 6A and 7A1–A4) and 2 h p.i., (Figures 6B and 7B1–B4) trophoblast cell line was confluent and very flat. At these time points, we observed bright round or oval particles with diameters in the 200–400 nm range at different locations: (i) intracellularly, (ii) attached to the edges of the cells on plasma membranes, and (iii) on top of the cells at the periphery or at the soma. The latter location coincided with plasma membrane slight pits below the particles, presumably sites of MPXV virions endocytosis. At 18 h p.i. (not shown) and 24 h p.i. (Figures 6C and 7C1–C4), cells' monolayers were found disorganized compared to earlier time points: cells formed more microvilli and some cells had a foamy appearance with numerous holes at the apical side. Amorphous materials were present on top or at cell periphery, and a lot of debris were present in the extracellular space. Among these debris, some MPXV-like particles were found. MPXV-like particles were also found on top of the placental cells, with round, elongated, or brick shapes (Figure 7C4). From 48 h (Figures 6D and 7D1–D4) to 72 h (Figures 6E and 7E1–E4) p.i., MPXV infected trophoblast cell line presented shrinked morphologies with cellular protrusions, and cellular contractions-induced holes in the cell monolayers. MPXV-like particles were observed at these time points at extracellular locations (Figure 7C2–D2) as well as on the soma or on lamellipodia of the placental cells (Figure 7C4–D4). At 96 h p.i., MPXV-infected placental cell monolayers were completely disorganized (Figure 6F), with the soma clearly distinct from peripheral cellular

FIGURE 3 First day time course of MPXV infection in trophoblast JEG3 cells. At 30 min postinfection time extracellular viruses (A1, zoom-in in A2) were found attached at the periphery of the cells (line arrows) in actin-rich regions. One-hour postinfection (p.i.) (B1, C1, zoomed-in views in B2, C2), MPXV-like particles were found in peripheral cellular regions, more centrally distributed. At 2 h p.i. time point, MPXV-like particles were found mixed with membranous material located inside intracytoplasmic vacuoles (D1, E1, F1, zoomed-in views in D2, E2, F2; line arrows). MPXV infected placental cells at 18 and 24 h p.i. time points. At 18 h p.i., mature MPXV particles (line arrows) depicted close to a nucleus (n.) (G1, G2 and H2) at the level of nuclear invagination (G1, zoomed-in views in H2). Immature MPXV particles (block arrows) were also present in the cell, but located more distantly from the nucleus (n.) (G2, zoomed-in view in H1). At 24 h p.i. time point (I1), mature (line arrows, I2) as well as immature (block arrows, J1) MPXV particles located in a cell at the level of a nuclear invagination, between actin-like microfilaments bundles (arrowheads). Example of similar ultrastructural organization depicted in another cell at 24 h p.i. (J2). MPXV, monkeypox virus.

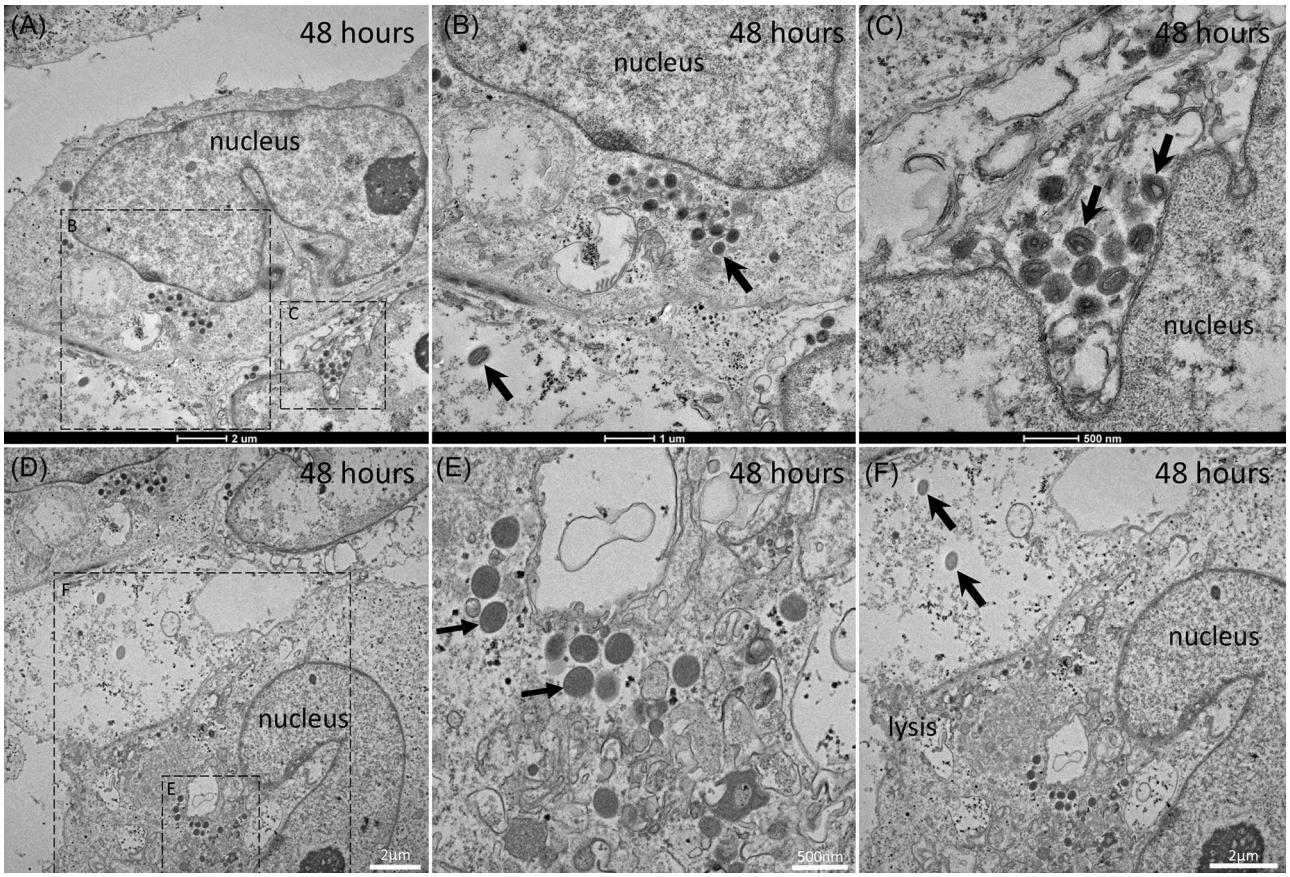

FIGURE 4 Second day time course of MPXV infection in trophoblast JEG-3 cells. MPXV infected placental cells at 48 h postinfection time point (A and D). Intracellular mature MPXV particles (line arrows, B, C, and F) located in two contacting cells (A and D), in well-preserved cytoplasmic regions (C) or lytic disorganized cytoplasmic regions (F). Intracellular dense immature MPXV particles were also present (D, zoomed-in view in E). MPXV, monkeypox virus.

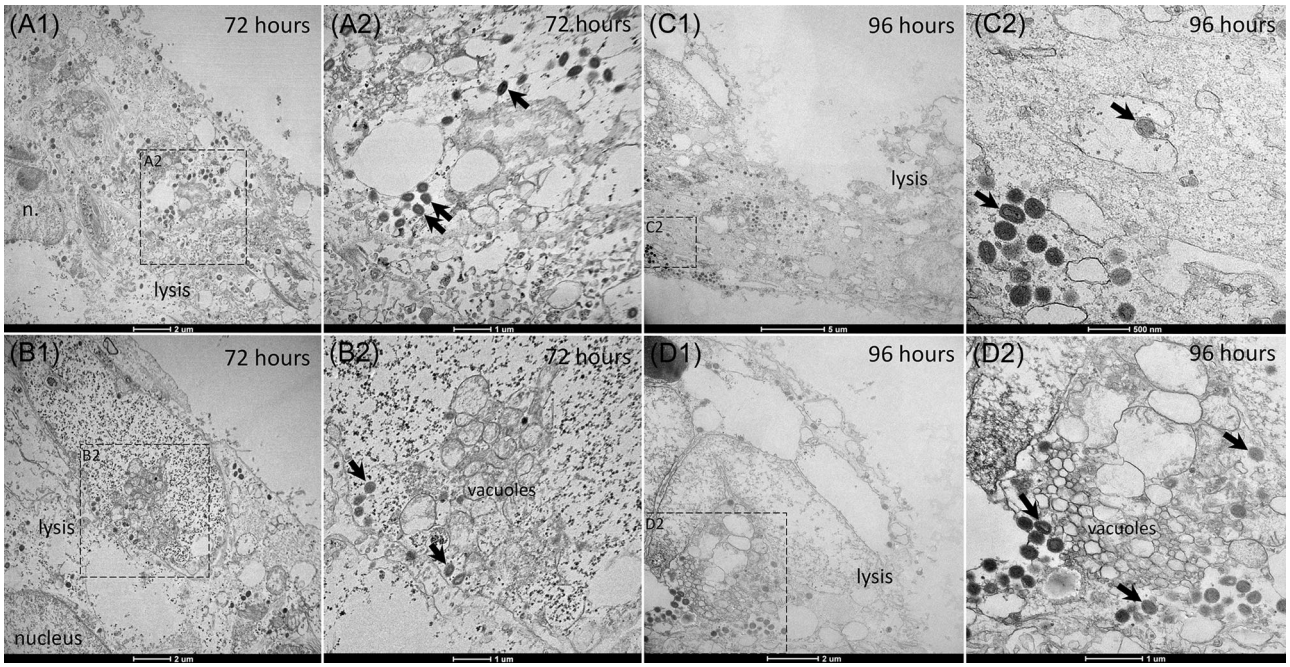

FIGURE 5 MPXV infected trophoblast JEG-3 cells at 72- and 96-h postinfection time points. At 72 h p.i., intracellular mature MPXV particles (line arrows, A2 and B2) located in two different lytic cells (A1 and B1) containing a disorganized cytoplasm rich in vacuoles. At 96 h p.i., intracellular mature MPXV particles (line arrows, C2 and D2) accumulated in lytic cells (C1 and D1) characterized by a disorganized cytoplasm enriched in vacuoles. MPXV, monkeypox virus.

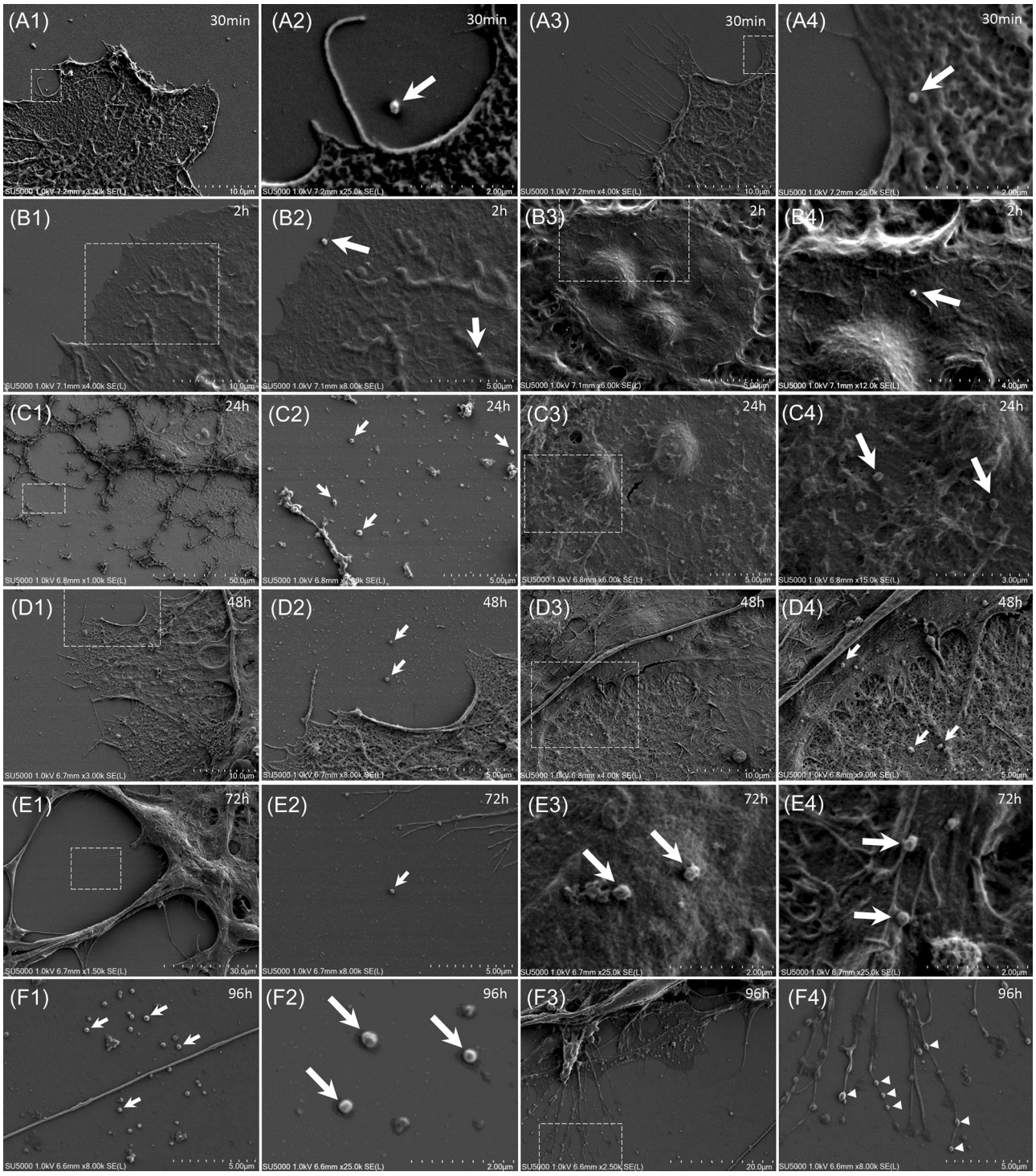

FIGURE 6 Scanning electron microscopy of whole-mount MPXV infected trophoblast JEG-3 cell monolayers. At 30 min (A), 2 h (B), 24 h (C), 48 h (D), 72 h (E), and 96 h (F) postinfection time points. MPXV-like particles (line arrows) were observed at extracellular and cellular locations. Ninety-six hours postinfection, plasma membrane swellings (arrowheads) were observed at the level of lamellipodia and filopodia of placental cells (F3 and F4). MPXV, monkeypox virus.

regions consisting in lamellipodia, filopodia, or amorphous lytic-like material. Multiple lamellipodia/filopodia-like formations with the presence of MPXV particles inside and at the tip were also observed after primary trophoblasts infection (Figure S9). Numerous MPXV-like particles with round, elongated, brick, or bullet shapes were depicted at extracellular locations, as well as on the whole cell bodies. Surprisingly, we noticed the presence of plasma membrane swellings at the level of lamellipodia and filopodia on the MPXV-infected JEG-3

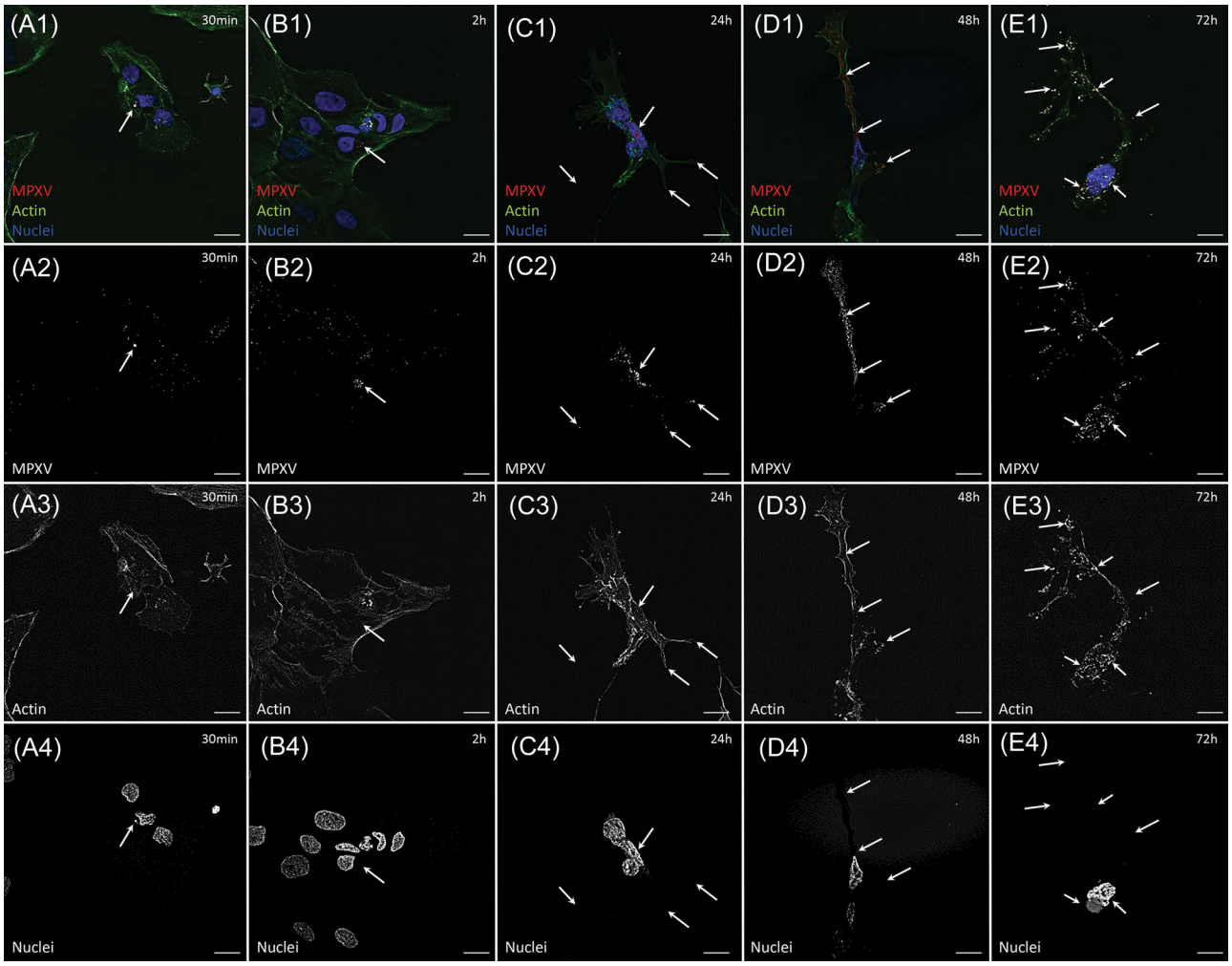

FIGURE 7 Confocal scanning light microscopy of MPXV-infected trophoblast JEG-3 cell monolayers. At 30 min (A1–A4), 2 h (B1–B4), 24 h (C1–C4), 48 h (D1–D4) and 72 h (E1–E4) postinfection. Arrows point to MPXV particles. MPXV, monkeypox virus.

cells (Figure 7F3–F4). These membrane swellings had a larger diameter than MPXV-like particles, eventually corresponding to MPXV virions trafficking in thin cellular regions before cell release.

To confirm and expand our SEM experiments, we performed confocal laser SEM of MPXV-immunostained JEG-3 cells. The cells were also stained for filamentous actin (F-actin) and nuclei (DAPI).

First, we confirmed the flattening of the JEG-3 cells monolayers, by measuring a thinning of the cell monolayers over the infectious time course, with a decrease in cells thickness from 3.8 to 1.8 µm from 30 min p.i. to 48 h p.i., respectively, as seen in orthogonal side views in the Z-stacks (data not shown; top views in Figure S8). Second, we confirmed the different cellular locations of the MPXV virus particles (Figure 8) and cell morphology characteristics (Figure S8) over the infection time course. Immunostained MPXV virions were observed for most of them at JEG-3 cells periphery 30 min p.i. (Figure 8A), or intracellularly 2 h p.i. (Figure 8B). From 24 h p.i., a larger and increasing amount of MPXV particles compared to early (30 min and 2 h) time points were present in the cells, coinciding with a stretching of the cells (Figure 8C and Figure S8). As in TEM ultra-thin sections images, some nuclear indentations around concentrations of MPXV virions were noticed in the fluorescence images (Figure S8D). Of note, the amount of MPXV immunostained particles was slightly more pronounced in isolated cells from the periphery of JEG-3 cells monolayers compared to more central regions of the monolayers, presumably because of an effect of the confluence on cells responsiveness to infection or because of antibodies access to the cells. Actin filaments from JEG-3 cells were found over the MPXV infection time course more densely packed along cell contours.

These experiments also confirmed our SEM finding with MPXV particles located in JEG-3 cells protrusions, as early as 24 h p.i.: MPXV particles were found located in cells soma but also in the tip of thin filopodia (Figure 8C). Single-plane analysis of our confocal Z-stacks confirmed the inner location of the virions regarding the filopodia. MPXV particles were thus located along the entire length of the infected JEG-3 and primary trophoblast cells and depending on the thickness of the cell's protrusions, particles were present. Eventually, for cells possessing very thin and long filopodia, particles

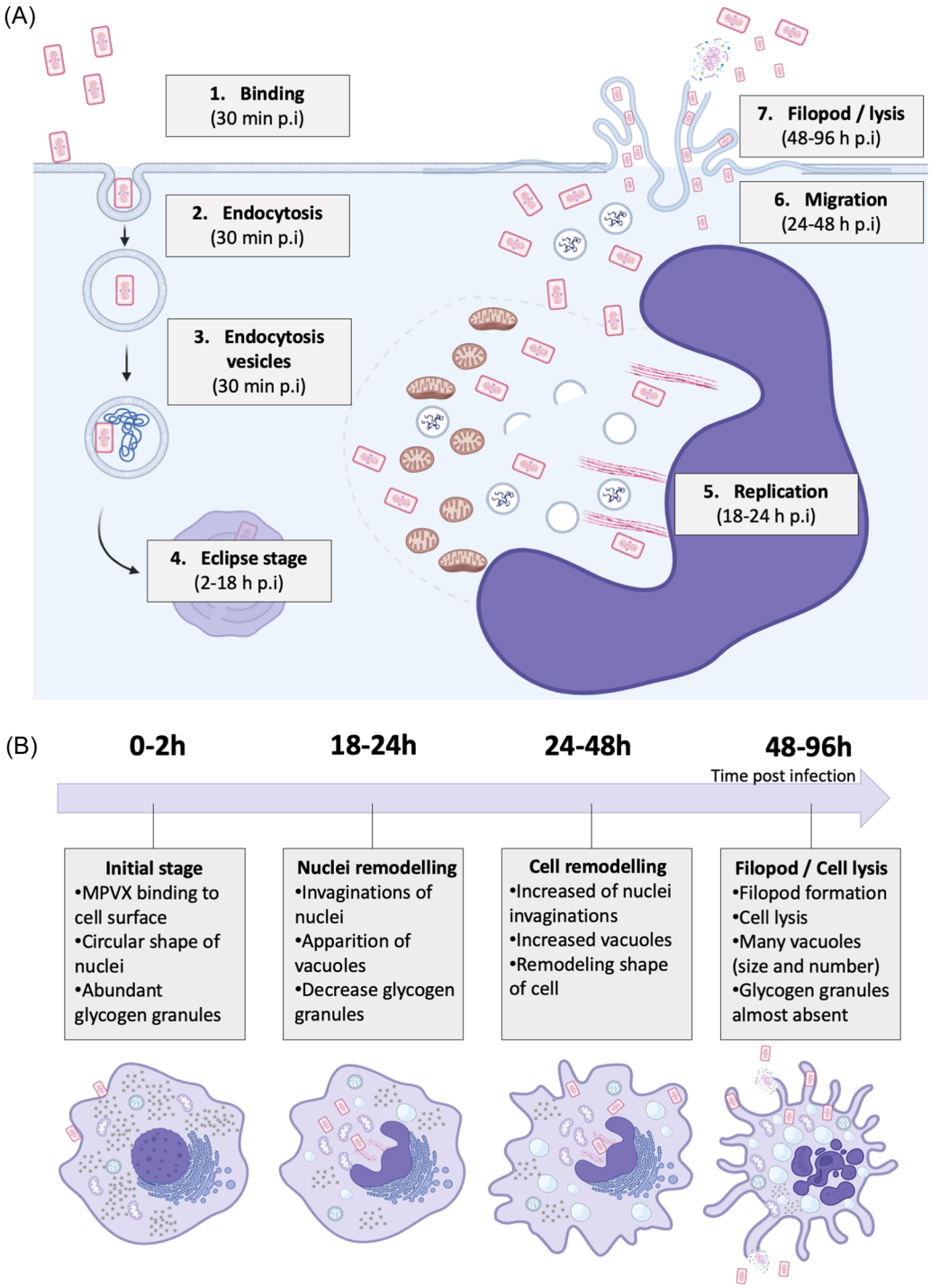

FIGURE 8 Graphical representation summarizing the main features of MPXV infection in trophoblast cells. (A) Summary of the key stages in the MPXV replication cycle in placental cells. In the early stages, viral particles attach to and are then endocytosed in vesicles, followed by an eclipse phase. During the replication phase, the nucleus in which the viral factory is located invaginates. Over time, the virus migrates toward the membrane and is released via filopodia. (B) Summary of specific MPXV modulations on placental cells. In the early stages, we observe a normal shape of the nucleus and cell, with an abundance of glycogen granules. As the virus replicates, the shape of the nucleus modulates, becoming more pronounced over time, with the appearance of more and more vacuoles. In the late stages, filopodia are formed, in which the virus becomes lodged and is then released. In the second stage, cell shrinkage leads to cell lysis. MPXV, monkeypox virus.

were located both close to the nucleus and at the tip of these cellular extensions, projecting MPXV particles far away from the cell's soma (Figure 8 and Figure S9).

4 | DISCUSSION

We demonstrate in the present in vitro study that trophoblasts represent a target for MPXV. Our results summarized in Figure 8 suggest that for vertical transmission of MPXV to the fetus in pregnant women, MPXV originating from the vagina or maternal bloodstream may infect placental syncytiotrophoblasts and further disseminate after virus replication and cell lysis.

Regarding the ultrastructural features of MPXV replication cycle in JEG-3 cells per se, our results show that MPXV replicates as in Vero E6 cells with the same virions assembly steps, but differences at two levels. First, regarding periods: MPXV uptake is slightly delayed in JEG-3 cells compared to Vero E6 cells, and the so-called "eclipse-phase" is slightly longer in JEG-3 cells compared to Vero E6 cells. Secondly, there are differences regarding the location of the newly formed MPXV particles in the cells. Indeed, if Vero E6 cells tend to remain round with a clear central versus peripheral location of immature versus mature particles, in contrast, JEG-3 cells stretch over MPXV infection time course, with MPXV immature and mature particles less clearly asymmetrically organized within the cells, which develop nuclear indentations and actin-filaments bundles.

Our results showing that there is a cellular remodeling of the syncytiotrophoblasts and a detachment of these cells from the villosities following long-term infection suggest that the loss of placenta integrity may facilitate viral spreading in MPXV-infected pregnant women.[29]

Also, we show that MPXV can locate in trophoblast cells filopodia, thus probably facilitating "budding," a common exit mechanism for viruses.[30] Virus propagation between cells via filopodia has been described in vitro for viruses belonging to different families, such as, for example, ectromelia (ECTV) orthopoxvirus,[31] Marburg filovirus,[32] or more recently SARS-CoV-2 virus.[33] Aforementioned viruses can use filopodia as guides once externalized by surfing on it, or can be moved inside filopodia before release. In our study, MPXV seem to preferentially use filopodia as budding sites, albeit surfing might also occur. Morphological changes of placental cells over MPXV infection time course, especially illustrated by the shrinking and thinning of the cell's monolayers, and the development of very long and thin cellular protrusions, reflect direct cytoskeleton rearrangements as seen with actin filaments staining. It may also reflect an indirect effect of infection relying on the disrupting of signaling(s) such as Rho-ROCK pathway and the acto-myosin system.[34] Such morphological changes may also appear in vivo in human placenta tissue and may help propagate MPXV dissemination and contribute to pregnancy problems by disrupting mother–fetus exchanges.[18,20,35,36]

Numerous viruses, such as rubella, measles virus, varicella-zoster virus (VZV), parvovirus B19 (PVB19), human cytomegalovirus (CMV), Zika virus, hepatitis E virus type 1 and 2, herpes simplex 1 and 2, human immunodeficiency virus and hepatitis A to C viruses can cause typical and/or atypical exanthemas such as MPXV.[37] In pregnant women, these viruses can also be transmitted to the fetus, eventually leading to pregnancy complications and fetal death, depending on the trimester of infection. The biology of viruses linked to congenital diseases, including newly discovered viruses and ones that were overlooked because they did not grow well in cell culture, is still largely unknown. How these viruses spread basal decidua through viremia, immune cell trafficking, or both is still unknown. Understanding inherent variations is necessary when studying complex human tissues, especially differentiated placentas, between individual donors and gestational ages.[37,38]

AUTHOR CONTRIBUTIONS

Jonatane Andrieu and Jean-Pierre Baudoin were involved in experimental design and execution, data analysis, writing paper, and figure generation. Jonatane Andrieu and Margaux Valade carry out viral infections as well as viral replication and cell viability. Marion Lebideau isolated and amplified the viral strain from the clinical isolate. Bernard La Scola provided virus strain and expertise. Nathalie Wurtz was in charge of regulatory aspects of the use of the virus and the safety of experiments in the BSL3 laboratory. Jean-Louis Mège and Florence Bretelle set up and carried out the administrative procedures for the cohort of pregnant patients to recover placentas. Soraya Mezouar supervised manuscript preparation and mentorship. Jean-Pierre Baudoin contributed expertise in the field of microscopy, guidance for experimental design, supervised the study, and manuscript preparation.

ACKNOWLEDGMENTS

The authors sincerely thank Takashi Irie, Kyoko Imai, Shigeki Matsubara, Yusuke Ominami, Akiko Hisada, and Hitachi High-Tech Corporation for the installation of the SU5000 microscope in our facility. The authors are also thankful to Dr. Jacques Bou Khalil for access to the scanning electron microscopy facility.

CONFLICT OF INTEREST STATEMENT

The authors declare no conflict of interest.

DATA AVAILABILITY STATEMENT

Not applicable. However, we can share high-resolution microscopy figures with the readership. Please contact the corresponding authors.

ORCID

Jonatane Andrieu http://orcid.org/0000-0002-3603-0426
Soraya Mezouar http://orcid.org/0000-0002-2285-7051
Bernard La Scola http://orcid.org/0000-0001-8006-7704

REFERENCES

1. Lum FM, Torres-Ruesta A, Tay MZ, et al. Monkeypox: disease epidemiology, host immunity and clinical interventions. *Nat Rev Immunol*. 2022;22(10):597-613.

2. Ciccarese G, Di Biagio A, Bruzzone B, et al. Monkeypox outbreak in Genoa, Italy: clinical, laboratory, histopathologic features, management, and outcome of the infected patients. *J Med Virol*. 2023; 95(2):e28560.
3. Carugno A, Parietti M, Ciccarese G, et al. Clinical-epidemiological aspects of the monkeypox 2022 epidemic: a multicentre study by the Italian SIDeMaST group of sexually transmitted, infectious and tropical diseases. *J Eur Acad Dermatol Venereol*. 2023;37(11): e1277-e1279.
4. Rodríguez-Cuadrado FJ, Nájera L, Suárez D, et al. Clinical, histopathologic, immunohistochemical, and electron microscopic findings in cutaneous monkeypox: a multicenter retrospective case series in Spain. *J Am Acad Dermatol*. 2023; 88(4):856-863.
5. Thornhill JP, Barkati S, Walmsley S, et al. Monkeypox virus infection in humans across 16 countries—April–June 2022. *N Engl J Med*. 2022;387(8):679-691.
6. Orviz E, Negredo A, Ayerdi O, et al. Monkeypox outbreak in Madrid (Spain): clinical and virological aspects. *J Infect*. 2022; 85(4):412-417.
7. Vaughan AM, Cenciarelli O, Colombe S, et al. A large multi-country outbreak of monkeypox across 41 countries in the WHO European Region, 7 March to 23 August 2022. *Euro Surveill*. 2022;27(36): 2200620.
8. Brown B, Fricke I, Imarogbe C, et al. Virus monkeypox et aperçu de ses protéines immunomodulatrices—Weaver—2008—Revues immunologiques. *Explor immunol*. 2023. Wiley Online Library [Internet]. [cited June 21, Wiley Online Library [Internet]. [cited June 21, http://onlinelibrary.wiley.com/doi/full/10.1111/j.1600-065X.2008.00691.x
9. Magnus P, Andersen EK, Petersen KB, Birch-Andersen A. A pox-like disease in cynomolgus monkeys. *Acta Pathol Microbiol Scand*. 1959;46(2):156-176.
10. Schmidle P, Leson S, Wieland U, Böer-Auer A, Metze D, Braun SA. Lives of skin lesions in monkeypox: histomorphological, immunohistochemical, and clinical correlations in a small case series. *Viruses*. 2023;15(8):1748.
11. Moltrasio C, Boggio FL, Romagnuolo M, et al. Monkeypox: a histopathological and transmission electron microscopy study. *Microorganisms*. 2023;11(7):1781.
12. Paniz-Mondolfi A, Reidy J, Pagani N, et al. Genomic and ultrastructural analysis of monkeypox virus in skin lesions and in human/animal infected cells reveals further morphofunctional insights into viral pathogenicity. *J Med Virol*. 2023;95(6):e28878.
13. Müller M, Ingold-Heppner B, Stocker H, Heppner FL, Dittmayer C, Laue M. Electron microscopy images of monkeypox virus infection in 24-year-old man. *Lancet*. 2022;400(10363):1618.
14. Witt ASA, Trindade GS, Souza FG, et al. Ultrastructural analysis of monkeypox virus replication in Vero cells. *J Med Virol*. 2023;95(2):e28536.
15. Heuser J. Deep-etch EM reveals that the early poxvirus envelope is a single membrane bilayer stabilized by a geodetic "honeycomb" surface coat. *J Cell Biol*. 2005;169(2):269-283.
16. Mandelbrot L, Vauloup-Fellous C, Huissoud C, Ghosn J, Picone O. Monkeypox: proposals for care in pregnancy. *Gynecol Obstet Fertil Senol*. 2023;51(5):284-288.
17. Delorme-Axford E, Donker RB, Mouillet JF, et al. Human placental trophoblasts confer viral resistance to recipient cells. *Proc Natl Acad Sci USA*. 2013;110(29):12048-12053.
18. Fuentes-Zacarías P, Murrieta-Coxca JM, Gutiérrez-Samudio RN, et al. Pregnancy and pandemics: interaction of viral surface proteins and placenta cells. *Biochim Biophys Acta Mol Basis Dis*. 2021; 1867(11):166218.
19. Zaucha GM, Jahrling PB, Geisbert TW, Swearengen JR, Hensley L. The pathology of experimental aerosolized monkeypox virus infection in cynomolgus monkeys (Macaca fascicularis). *Lab Invest*. 2001;81(12):1581-1600.
20. Dashraath P, Alves MP, Schwartz DA, Nielsen-Saines K, Baud D. Potential mechanisms of intrauterine transmission of monkeypox virus. *Lancet Microbe*. 2023;4(1):e14.
21. Schwartz DA, Ha S, Dashraath P, Baud D, Pittman PR, Adams Waldorf KM. Mpox virus in pregnancy, the placenta, and newborn. *Arch Pathol Lab Med*. 2023;147(7):746-757.
22. Kupper N, Pritz E, Siwetz M, Guettler J, Huppertz B. Placental villous explant culture 2.0: flow culture allows studies closer to the in vivo situation. *Int J Mol Sci*. 2021;22(14):7464.
23. Miller RK, Genbacev O, Turner MA, Aplin JD, Caniggia I, Huppertz B. Human placental explants in culture: approaches and assessments. *Placenta*. 2005;26(6):439-448.
24. Bayer A, Lennemann NJ, Ouyang Y, et al. Type III interferons produced by human placental trophoblasts confer protection against Zika virus infection. *Cell Host Microbe*. 2016;19(5): 705-712.
25. Le Bideau M, Wurtz N, Baudoin JP, La Scola B. Innovative approach to fast electron microscopy using the example of a culture of virus-infected cells: an application to SARS-CoV-2. *Microorganisms*. 2021;9(6):1194.
26. Cai J, Peng T, Wang J, et al. Isolation, culture and identification of choriocarcinoma stem-like cells from the human choriocarcinoma cell-line JEG-3. *Cell Physiol Biochem*. 2016;39(4): 1421-1432.
27. Cao H, Lei ZM, Bian L, Rao CV. Functional nuclear epidermal growth factor receptors in human choriocarcinoma JEG-3 cells and normal human placenta. *Endocrinology*. 1995;136(7):3163-3172.
28. Olivier E, Wakx A, Fouyet S, Dutot M, Rat P. JEG-3 placental cells in toxicology studies: a promising tool to reveal pregnancy disorders. *Anat Cell Biol*. 2021;54(1):83-92.
29. Heerema-McKenney A. Defense and infection of the human placenta. *APMIS*. 2018;126(7):570-588.
30. Chang K, Baginski J, Hassan SF, Volin M, Shukla D, Tiwari V. Filopodia and viruses: an analysis of membrane processes in entry mechanisms. *Front Microbiol*. 2016;7:300.
31. Szulc-Dąbrowska L, Gregorczyk-Zboroch KP, Struzik J, et al. Long actin-based cellular protrusions as novel evidence of the cytopathic effect induced in immune cells infected by the ectromelia virus. *Cent Eur J Immunol*. 2018;43(4):363-370.
32. Schudt G, Kolesnikova L, Dolnik O, Sodeik B, Becker S. Live-cell imaging of Marburg virus-infected cells uncovers actin-dependent transport of nucleocapsids over long distances. *Proc Natl Acad Sci USA*. 2013;110(35):14402-14407.
33. Zhang Y, Zhang X, Li Z, et al. Single particle tracking reveals SARS-CoV-2 regulating and utilizing dynamic filopodia for viral invasion. *Sci Bull*. 2023;68(19):2210-2224.
34. Sit ST, Manser E. Rho GTPases and their role in organizing the actin cytoskeleton. *J Cell Sci*. 2011;124(pt 5):679-683.
35. Mbala PK, Huggins JW, Riu-Rovira T, et al. Maternal and fetal outcomes among pregnant women with human monkeypox infection in the democratic Republic of Congo. *J Infect Dis*. 2017;216(7): 824-828.
36. Schwartz DA, Ha S, Dashraath P, Baud D, Pittman PR, Waldorf KA. Monkeypox virus in pregnancy, the placenta and newborn: an emerging poxvirus with similarities to smallpox and other orthopoxvirus agents causing maternal and fetal disease. *Arch Pathol Lab Med*. 2023;11(8):1345.
37. Pereira L. Congenital viral infection: traversing the uterine-placental interface. *Annu Rev Virol*. 2018;5(1):273-299.

38. Malik S, Ahmed A, Ahsan O, Muhammad K, Waheed Y. Monkeypox virus: a comprehensive overview of viral pathology, immune response, and antiviral strategies. *Vaccines*. 2023;11(8):1345.

SUPPORTING INFORMATION

Additional supporting information can be found online in the Supporting Information section at the end of this article.

How to cite this article: Andrieu J, Valade M, Lebideau M, et al. Pan-microscopic examination of monkeypox virus in trophoblasts cells reveals new insights into virions release through filopodia-like projections. *J Med Virol*. 2024;96:e29620. doi:10.1002/jmv.29620